DESIGN AND IMPLEMENTATION OF INTELLIGENT PROTECTION SYSTEM FOR CHARGING DEVICE OF NEW ENERGY VEHICLE

Di Zheng[1], Baobao Zheng[2]*
[1]Xinyang Vocational and Technical College, Xinyang 464000, China
[2]Xinyang Vocational College of Arts, Xinyang 464000, China

Abstract - The charging device of new energy vehicles faces safety risks such as over-temperature, over-voltage, insulation failure, etc. The traditional passive protection mode can not realize early warning and active intervention of faults. The intelligent protection system of charging device, data acquisition, fault diagnosis and classified protection are designed and implemented. A charging simulation experiment platform was built, and five kinds of parameters such as charging gun head temperature, radiator temperature, ambient temperature, DC current and DC voltage were collected at a sampling frequency of 1kHz, and 4,500 sets of sample data sets were constructed for normal state and five kinds of faults such as overtemperature, overvoltage, undervoltage, insulation and communication. An improved convolutional neural network model integrating channel attention mechanism is proposed, and the attention module is introduced after the convolution layer to weight the sensor channels. The accuracy of the model test set is 97.2%, and the F1 score is 96.8%, which is 2.5 and 2.7 percentage points higher than the standard convolutional neural network. The system is deployed in the edge computing terminal of Raspberry Pie CM4. The single diagnosis period is 237 milliseconds, the response of primary protection (down to 48A) is 57 milliseconds, and the response of secondary protection (circuit cut) is 8.3 milliseconds. The accuracy rate is 92.1% in the noise environment with signal-to-noise ratio of 10dB. The hierarchical protection strategy realizes active intervention in the process of charging gun head temperature rise, and controls the peak temperature below 95℃. The system is suitable for three scenarios: public fast charging station, residential area slow charging pile and expressway service area, and provides technical solutions for active protection of charging facilities.

Keywords: New energy vehicles; Charging device; Intelligent protection system; Convolutional neural network.

1. Introduction

The new energy automobile industry has entered a stage of rapid development. By the end of 2025, the number of new energy vehicles in China has exceeded 40 million, and the number of charging piles has increased to more than 15 million. As the key infrastructure of energy supply, the operation safety of charging device affects vehicle use and public safety. Over-temperature, over-voltage, and insulation failures caused by aging interfaces, power grid fluctuations, and excessive ambient temperature occur from time to time during charging. In 2023, there were more than 300 publicly reported charging fire accidents, which revealed that the current charging equipment was insufficient in early warning and active protection of failures. Unlike petrol or diesel vehicles, where the stored chemical energy can only be released under suitable environmental conditions (e.g., proper air–fuel ratio and ignition source), electric vehicle batteries contain both fuel and oxidizer internally. Once a thermal runaway occurs due to over-temperature, over-voltage, or insulation failure, the fire cannot be extinguished by conventional methods; the most effective countermeasure is to submerge the entire vehicle in water, converting the released heat into water vapour. This does not eliminate the fault but merely contains its effects. Therefore, any intelligent system that can predict catastrophic failures before they happen – such as the one proposed in this work – is of great practical utility for reducing fire accidents and improving charging safety.

dx.doi.org/10.17683/ijomam/issue24.15

The traditional protection mechanism relies on passive components such as fuses and circuit breakers, and the circuit can only be cut off after the fault occurs, so it is impossible to predict the risk in advance. Building a protection system with real-time monitoring, intelligent diagnosis and automatic disposal capabilities has become a path to improve the safety level of charging. The introduction of data-driven method into the field of fault identification of charging devices is helpful to shorten the fault response time, reduce the false alarm rate and provide technical support for the transformation of charging facilities from passive protection to active protection.

In the field of safety protection of charging facilities, rich achievements have been accumulated around the protection strategy of microgrid and smart substation. Peter et al. (2025) summarized the intelligent protection strategies for microgrid. Distributed energy access challenges the traditional protection scheme, and the intelligent protection system needs to have adaptive and cooperative capabilities [1]. Zhu et al. (2025) put forward the technical scheme of relay protection and safety for the expansion project of smart substation, emphasizing the reliability and quick response characteristics of the protection system under complex working conditions [2]. Esfahani and Mohammed (2020) developed a protection scheme to deal with extreme fault current in smart power system, and adopted intelligent algorithm to realize rapid identification and isolation of fault current [3]. Samonto et al. (2020) constructed a cascade intelligent fault protection model of fuzzy logic, and introduced fuzzy reasoning into the decision-making process of relay protection [4]. Achou et al. (2020) induction motor protection system based on Sugeno reasoning provides an application example of fuzzy logic for electrical equipment fault diagnosis [5]. In terms of charging device and energy management, Cao et al. (2025) studied flexible wireless charging energy storage devices, focusing on energy conversion efficiency and thermal management during charging [6]. Bae (2023) analyzed the resonance characteristics of LLC resonant converter for fast charging of smart batteries of personal mobile devices, and found that there was a coupling relationship between frequency and temperature during charging [7]. Kok et al. (2024) designed a new portable solar wireless charging device, which verified the running stability of charging equipment in outdoor environment [8]. Liu et al. (2021) proposed a mobile device charging algorithm based on reinforcement learning, and introduced intelligent decision-making into charging process control [9]. Pröbstl et al. (2020) Intelligent charger can prolong the service life of mobile devices by optimizing charging strategy, and emphasizes the importance of charging management algorithm for device safety [10]. In terms of the layout of new energy vehicles and charging facilities, Xiao et al. (2024) constructed a weighted network model of charging stations for new energy vehicles, and analyzed the influence of the layout structure of charging stations on operating efficiency [11]. Wang et al. (2023) developed an electronic parking algorithm for new energy vehicles based on fuzzy model predictive control, demonstrating the application potential of intelligent algorithm in the field of vehicle control [12]. Ma et al. (2025) analyzed the linkage relationship between China's new energy automobile industry and Tesla from the perspective of capital market, and pointed out that the rapid development of the industry put forward higher requirements for supporting infrastructure [13]. In terms of data security and intelligent identification, Meng and Wen (2025) based on the privacy protection algorithm of intelligent data identification provided technical reference for data security of charging system [14]. Wang (2025) Intelligent networked automobile data security protection method based on distributed remote network information management system, emphasizing data protection in the process of vehicle-pile communication [15]. Dziech and Mees (2022) discussed the intelligent multimedia system for threat detection and data protection, and its data security concept can be used for reference in charging protection system [16].

In terms of user behavior and industrial policy, Zhao et al. (2024) empirically studies the acceptance of new energy vehicles from the perspective of female consumers, and users pay high attention to charging safety [17]. Sun and Ju (2023) Research on Multi-source Heterogeneous Data Promotion of New Energy Vehicles, from the dual perspectives of consumers and manufacturers [18]. Lv and Li (2021) predicted the output of new energy passenger cars under the background of double integral policy, and the industrial scale expanded rapidly driven by the policy [19]. Shen et al. (2021) analyzed the policy effect of new energy vehicles, and pointed out that policy guidance promoted technological progress and safety standards [20]. Mao et al. (2020) studied the influence of ocean power generation technology on the evolution of energy demand of new energy vehicles, and discussed the matching between energy supply end and charging demand end [21]. Zhang and Cai (2020) studied the subsidy strategy of

new energy vehicles based on incomplete information, and analyzed the market incentive mechanism from the perspective of economics [22].

The research focuses on the intelligent protection system of charging device, including data acquisition, fault modeling, system implementation and field verification.

In the data acquisition part, a temperature sensor, a Hall current sensor and a voltage detection module are distributed in the charging pile, and the sampling frequency is set to 1kHz, so as to collect four kinds of parameters, such as charging gun head temperature, three-phase input voltage, DC output current and ambient temperature. In the fault modeling part, a fault diagnosis model based on improved convolutional neural network and attention mechanism is constructed, and five typical faults such as overtemperature, overvoltage, undervoltage, communication interruption and insulation abnormality are identified, and the confidence score is output. In the system implementation part, the edge computing terminal based on ARM architecture is developed, the trained model is deployed, and the hierarchical protection strategy is designed: when the confidence is higher than 85%, the active flow reduction is triggered, and when it is higher than 95%, the power-off protection is implemented. The purpose of this study is to establish an intelligent protection system integrating data acquisition, edge diagnosis and classified protection. The average response time of fault identification is controlled within 200 milliseconds, and the accuracy of typical fault identification is over 97%, thus reducing the safety risks caused by charging faults.

The method of combining experimental verification with simulation is adopted. The first step is to build a data acquisition platform for the charging device. PT100 temperature sensor, ACS712 current sensor and ZMCT103C voltage transformer are selected, and STM32F407 main control chip is used to complete data acquisition and serial upload. The second step is to build a fault data set, and simulate five fault scenarios in the laboratory environment. Each scenario collects 1000 sets of samples, which are divided into training set, verification set and test set according to the ratio of 7:1.5:1.5. In the third step, a fault diagnosis model is established, local features are extracted by convolutional neural network, attention mechanism is introduced to assign weights to different sensor channels and Adam optimizer is used to update parameters, and the initial learning rate is set to 0.001. The fourth step is model evaluation, in which accuracy, precision, recall and F1 score are used as evaluation indexes, and compared with support vector machine, standard convolutional neural network and long-term and short-term memory network. The fifth step is to develop an embedded protection terminal. The trained model is converted into TensorFlow Lite format and deployed in Raspberry Pie CM4 module.

It communicates with the charging pile controller through Modbus RTU protocol to test the system response time and mis-operation frequency under different load conditions.

2. Materials and Methods

2.1 Data Collection and Sample Selection

To realize the data acquisition function described in the system overview, the following subsection details the specific data sources and the collection method.

2.1.1 Data Sources and Collection Methods

Experimental data source: Self-built charging device simulation experimental platform. The platform consists of a 60kW DC charging pile, a set of ternary lithium battery packs and a data acquisition unit. The charging pile outputs rated voltage of 500V and rated current of 120A. The data acquisition unit selects STM32F407 as the main controller, mounts three PT100 platinum resistance temperature sensors, and arranges the metal terminals inside the charging gun head, the power module heat sink inside the charging pile and the ambient air respectively. ACS712 linear Hall current sensor is used for current detection, and the range is set to 200 A, and the output voltage range is 0.5V to 4.5V. The voltage detection adopts ZMCT103C voltage transformer, and the primary input of 0 to 500V corresponds to the secondary output of 0 to 5 V. All sensor signals are collected by a 12-bit analog-to-digital converter in the main controller, and the sampling frequency is fixed at 1kHz. The collected data is uploaded to the local server for storage at the speed of 1000 pieces per second through the serial port to Wi-Fi module, and each piece of data contains six fields: time stamp, gun head temperature value, heat sink temperature value, environmental temperature value, DC current value and DC voltage value, as shown in Figure 1.

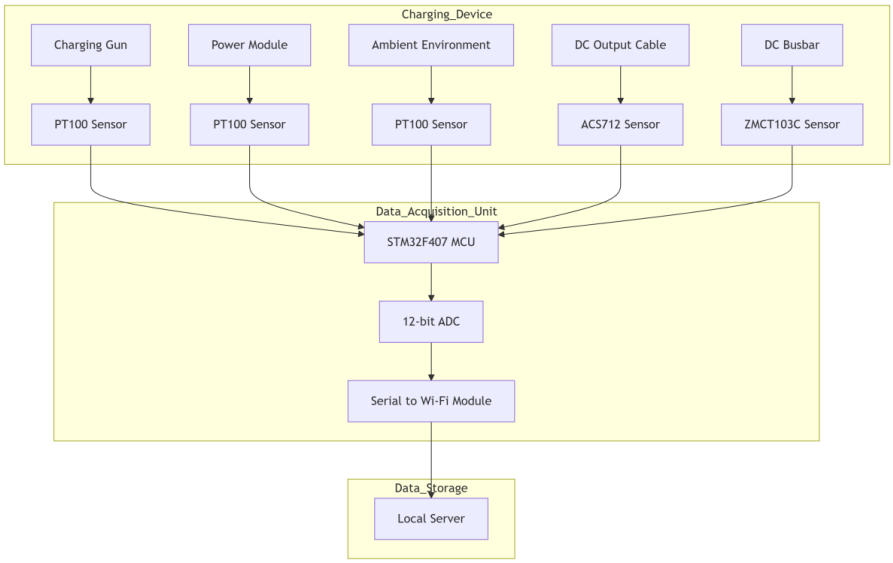

Figure 1: A topology diagram of a data acquisition system of a charging device

2.1.2 Sample Selection and Description

The experimental samples come from the operation data of the platform for 30 consecutive days. The normal samples were taken from the operation records of the charging pile under the conditions of output current of 30A to 100A and ambient temperature of 15℃ to 35℃, and 2000 groups were collected, each group of data contained 10,000 sampling points in 10 seconds. Fault samples are obtained by artificial simulation. The over-temperature fault was realized by wrapping the charging gun head with a heating sheet. When the gun head temperature exceeded 85℃, it was recorded, and 500 sets were collected. Over-voltage fault is recorded when the input voltage is raised to 110% of the rated value by the voltage regulator, that is, 550V, and 500 sets are collected. Under-voltage fault reduces the voltage to 85% of the rated value through the voltage regulator, and records at 425V, collecting 500 groups. Insulation failure is simulated by connecting 50 kω resistor between the positive and negative poles of DC output, and 500 sets are collected. The communication fault was simulated by interrupting the serial data stream, and 500 groups were collected. There are 2000 normal samples and 500 fault samples in each category, forming a data set with a total sample size of 4500 groups. Each group of samples is labeled with corresponding status labels, with normal status labeled as 0, overtemperature labeled as 1, overvoltage labeled as 2, undervoltage labeled as 3, insulation fault labeled as 4 and communication fault labeled as 5, as shown in Table 1.

Table 1. Sample distribution of the experimental data set

State Category	Sample Size (Groups)	Label Index	Sample Proportion (%)
Normal State	2000	0	44.4
Overheat Fault	500	1	11.1
Overvoltage Fault	500	2	11.1
Undervoltage Fault	500	3	11.1
Insulation Fault	500	4	11.1
Communication Fault	500	5	11.1
Total	4500	-	100.0

2.1.3 Data Preprocessing and Cleaning

Dimensional differences of different sensors and random noise interference in the original collected data. The temperature data is in degrees Celsius, ranging from -20℃ to 120℃. Current data unit ampere, ranging from -200A to 200A. The voltage data is in volts, ranging from 0V to 600V. Direct input of data with different dimensions into the model will lead to unbalanced gradient update, so it should be normalized. Maximum-minimum normalization method is used to map all features to [0,1] interval. Normalization formula as (1):

$$x' = \frac{x - \min(x)}{\max(x) - \min(x)} \tag{1}$$

In Formula (1), x represents the numerical value of a sampling point in the original data sequence, $\min(x)$ represents the minimum value of all samples in this feature dimension, $\max(x)$

represents the maximum value of all samples in this feature dimension, and x' represents the normalized numerical value, ranging from 0 to 1. For current and voltage channels, the minimum value is negative range, and the maximum value is positive range. For the temperature channel, the minimum value is -20℃ and the maximum value is 120℃.

There is high frequency noise, source electromagnetic interference and quantization error of analog-to-digital conversion in the original signal. The moving average filtering method is used for denoising, and the window width is set to 5. Take the arithmetic average of five consecutive sampling points as the filtered output value at the current moment. Figure 2 is a comparison between the original signal and the waveform after filtering and denoising.

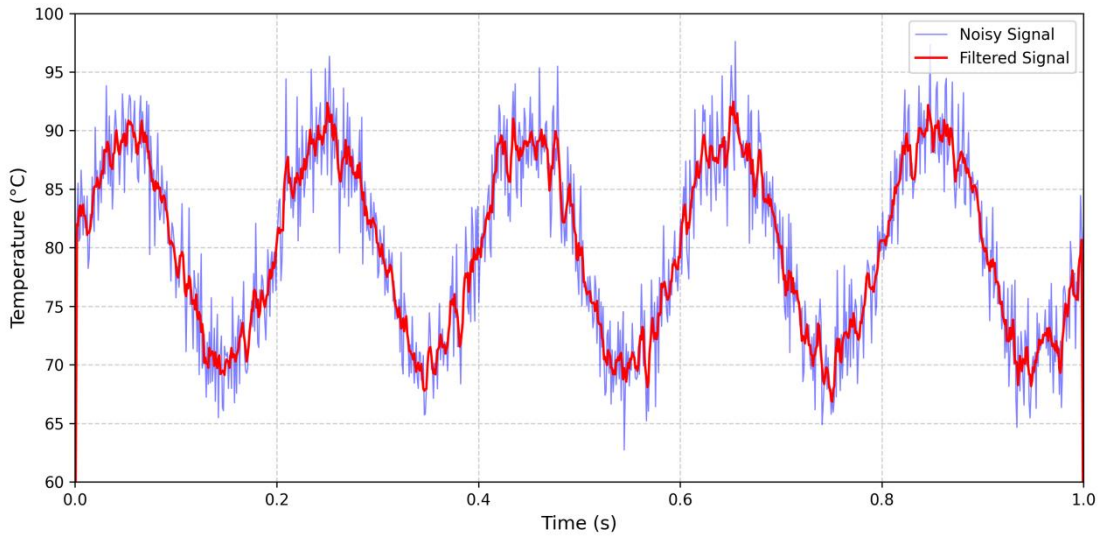

Figure 2: Comparison between the original signal and the waveform after filtering and denoising

2.2 Fault Diagnosis Model Selection and Construction

With the preprocessed dataset available, a fault diagnosis model must be designed. The architecture of the proposed improved convolutional neural network is presented below.

2.2.1 Improved Convolutional Neural Network Architecture Design

The model is based on convolutional neural network, and the input layer receives six channels of data, corresponding to six characteristic dimensions: gun head temperature, heat sink temperature, ambient temperature, DC current, DC voltage and time stamp. As shown in Figure 3, each input sample contains 200 data points in a row, forming a 200×6 input matrix.

The first layer convolution kernel size is set to 3×3, the number is 32, the step size is 1, and the ReLU activation function is adopted. The second layer convolution kernel size is also 3×3, the number is 64, and the step size is 1. After convolution, each layer is connected to the 2×2 maximum pool layer to compress the feature dimension. After the pooling operation, the feature map is flattened into a one-dimensional vector and input into the fully connected layer. The fully connected layer contains 128 neurons, followed by the Dropout layer, and the discard rate is set to 0.3, which inhibits overfitting. The number of neurons in the output layer is 6, which corresponds to the normal state and five kinds of fault States. The Softmax function is used to output the probability distribution of each category. The total number of parameters in the model is about 680,000. Using Adam optimizer, the initial learning rate is set to 0.001.

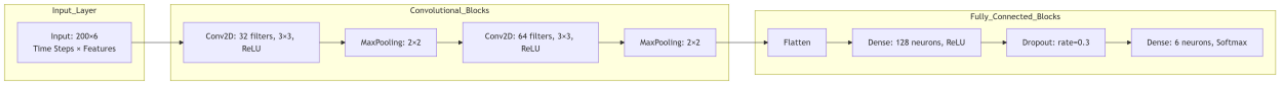

Figure 3: Overall architecture diagram of intelligent protection system model

2.2.2 Feature Weighting based on Attention Mechanism

Enhance the recognition ability of the model to the importance of different sensor channels, and introduce the channel attention module after the convolution layer. The module carries out global average pooling on the feature map output by convolution layer, and the global description vector of each channel is followed by two fully connected layers to learn the channel weights. The number of neurons in the first fully connected layer is 1/16 of the number of channels. ReLU activation function is

used, and the output number of the second fully connected layer is consistent with the number of channels. Sigmoid activation function is used to generate normalized weight coefficients. The calculation formula 3 of attention mechanism is as (2):

$$\text{Attention}(Q,K,V)=\text{softmax}\left(\frac{QK^T}{\sqrt{d_k}}\right)V \quad (2)$$

Q represents the query matrix, and the dimension $n\times d_k$, n is the sequence length, and d_k is the dimension of the query vector. K represents the bond matrix with dimension $n\times d_k$. V represents the value matrix, and the dimensions of $n\times d_v$ and d_v value vectors. $\sqrt{d_k}$ scaling factor, to prevent the gradient from entering the saturation region due to too large dot product result. The softmax function normalizes the dot product result into a probability distribution. Q, K and V all come from the same mapping of the output characteristic graph of convolution layer, forming a self-attention mechanism. The calculated weight coefficient is multiplied by the original feature map channel by channel to strengthen the contribution of important feature channels.

2.2.3 Loss Function and Optimization Strategy

The model uses classification cross entropy as the loss function to measure the difference between the predicted probability distribution and the real label. Equation 3 of the cross entropy loss function is as (3):

$$L=-\frac{1}{N}\sum_{i=1}^{N}\sum_{c=1}^{M}y_{i,c}\log(p_{i,c}) \quad (3)$$

N represents the number of samples in a batch, and the batch size is set to 64. M represents the total number of categories, with a value of 6. i represents the sample index, and its value ranges from 1 to N. c stands for category index, with values ranging from 1 to M. $y_{i,c}$ is indicator function, and the value is 1 when the real label of the i the sample belongs to the c class, otherwise it is 0.

The $p_{i,c}$ model predicts the probability that the i the sample belongs to the c the class, which is calculated by the output layer Softmax function. Adam optimizer is selected as the optimization strategy, and the initial learning rate is set to 0.001, the attenuation coefficient of first moment estimation β_1 is 0.9, the attenuation coefficient of second moment estimation β_2 is 0.999, and the numerical stability term ὸ is 10^{-8}. In the training process, the early stop mechanism is adopted, and the training is stopped when the loss of verification set does not decrease for 10 consecutive rounds.

2.3 Model Evaluation and Verification

Once the model is constructed and trained, its performance needs to be quantified using standard metrics. The definitions of these evaluation indicators are given in the next subsection.

2.3.1 Definition of Evaluation Indicators

The model performance evaluation selects four indicators: accuracy, precision, recall and F1 score. The calculation formula of accuracy is the proportion of correctly classified samples to the total number. The accuracy rate is calculated separately for each category, which is defined as the ratio of the number of samples predicted as this category and correctly predicted to all the samples predicted as this category. The recall rate is defined as the ratio of the number of samples predicted to be in this category and correctly predicted to the total number of real samples in this category. F1 score takes the harmonic average of accuracy and recall, and comprehensively measures the performance of the model in various categories.

As a basic statistical tool, the confusion matrix records the number of each type of sample predicted as each category. Macro-average refers to the direct arithmetic average of the index values of various categories, regardless of the imbalance of category samples. Weighted average takes the number of samples in each category as the weight to calculate the average value of indicators, as shown in Table 2.

Table 2. Model evaluation index system

Metric Name	Calculation Formula	Calculation Method	Value Range
Accuracy	(TP+TN)/(TP+TN+FP+FN)	Overall	[0,1]
Precision	TP/(TP+FP)	Per class Macro Weighted	[0,1]
Recall	TP/(TP+FN)	Per class Macro Weighted	[0,1]
F1 Score	2×Precision×Recall/(Precision+Recall)	Per class Macro Weighted	[0,1]

2.3.2 Comparative Experimental Setup

Verify the validity of the model and set up four groups of comparison models. In the first group of standard support vector machines, the kernel function is radial basis function, and the penalty coefficient c is set to 1.0. In the second group, the number of neurons in the hidden layer is 64, 128 and 64 respectively, and the input sequence length is fixed at 200. The third group of standard convolutional neural networks has the same structure as the improved model but does not include attention module. The fourth group of improved models, convolutional neural networks with channel attention mechanism. All models use the same data set division method, and the training set, verification set and test set are divided according to the ratio of 7:1.5:1.5. There are 3150 samples in the training set, 675 samples in the verification set and 675 samples in the test set. The training rounds are uniformly set to 100 rounds, and the early stop mechanism monitors the loss of the verification set, and terminates the training if it does not descend for 10 rounds in a row.

The same random seeds are used in the training of each model to ensure the reproducibility of the results, as shown in Figure 4.

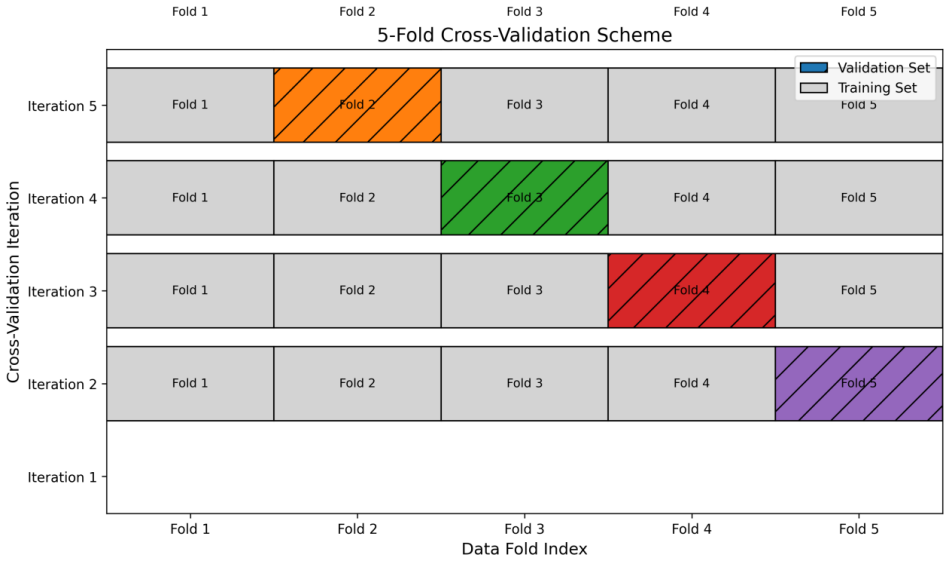

Figure 4: Schematic diagram of K-fold cross-validation (K=5)

2.4 System Implementation and Experimental Design

Having selected and validated the fault diagnosis model, the next step is to implement the complete intelligent protection system on physical hardware. The following subsections describe the hardware platform, communication protocols, software architecture, and experimental configuration.

2.4.1 Hardware Platform and Communication Protocol

The hardware platform of intelligent protection system consists of edge computing terminal, sensor acquisition unit and execution control unit. The edge computing terminal selects Raspberry Pie CM4 computing module, equipped with Broadcom BCM2711 quad-core processor, clocked at 1.5GHz, with a memory capacity of 4GB and built-in 32GB eMMC storage. The USB interface of the terminal is connected with the serial server and communicates with the data acquisition unit. The sensor acquisition unit follows the STM32F407 main control board described in section 2.1.1, and is equipped with PT100 temperature sensor, ACS712 current sensor and ZMCT103C voltage transformer, and the sampling frequency is fixed at 1kHz. The executive control unit is a solid-state relay, SSR-40DA, with rated load current of 40A, control voltage of 3-32V DC and response time of less than 10ms. The communication between the edge computing terminal and the charging pile controller is based on Modbus RTU protocol, and the physical layer is RS485 bus. The baud rate is set to 115200bps, with 8 data bits, 1 stop bit and no check bit. The terminal sends a status inquiry instruction to the charging pile controller every 50 milliseconds to read the running status code of the charging pile. When the fault confidence of the diagnosis model exceeds the threshold, the terminal outputs a high-level signal through the GPIO pin to drive the solid-state relay to cut off the charging loop. The overall power consumption of the hardware platform is controlled within 12W, which adapts to the power supply conditions of outdoor charging piles.

It should be emphasized that the Raspberry Pi CM4 is a prototyping platform chosen for its

flexibility, extensive software support, and low development cost. For industrial deployment in outdoor charging piles, an industrial-grade edge computing module (e.g., NVIDIA Jetson Xavier NX or Rockchip RK3588) with extended temperature range (-40°C to 85°C) and built-in hardware watchdog is recommended. The prototype described here serves as a proof of concept, and the same software pipeline can be ported to industrial hardware with minimal modifications.

2.4.2 Software Architecture and Functional Modules

The system software is designed with hierarchical architecture, which is divided into five levels from top to bottom: data acquisition layer, data processing layer, diagnosis and analysis layer, decision execution layer and data management layer. The data acquisition layer runs STM32F407 main control chip, which is responsible for sensor signal acquisition and serial port upload. The acquisition code is written in C language, and the analog-to-digital conversion results are carried by DMA to reduce CPU occupation. The data processing layer runs in Raspberry Pie CM4 and is developed in Python language, which is responsible for receiving the original data, performing sliding window splicing and normalization. The diagnosis and analysis layer loads the model trained in Section 2.2. The model is deployed in TensorFlow Lite format, with an input dimension of 200×6, and reasoning takes about 35 milliseconds at a time. The decision execution layer contains hierarchical protection logic. When the failure probability of model output exceeds 85%, the terminal sends a current reduction instruction to the charging pile controller to limit the output current to 60% of the rated value. When the failure probability exceeds 95%, the terminal triggers the solid-state relay to cut off the main circuit. The data management layer uses SQLite database to store running logs, each record contains time stamp, six-channel raw data, model output probability and execution action. The storage capacity is planned to be about 200MB per day, and the data will be automatically overwritten after 30 days of local retention, as shown in Figure 5.

To ensure system robustness against software hangs or infinite loops, a hardware watchdog timer is implemented. The Raspberry Pi CM4's onboard watchdog (BCM2711's hardware watchdog) is configured with a timeout period of 2 seconds. The diagnostic main loop sends a "keep-alive" signal (writing to /dev/watchdog) after each successful inference and decision cycle. If the loop stalls due to software fault or resource exhaustion, the watchdog triggers a hardware reset within 2 seconds, restoring the system to a known safe state. The watchdog status is logged in the SQLite database for post-event analysis.

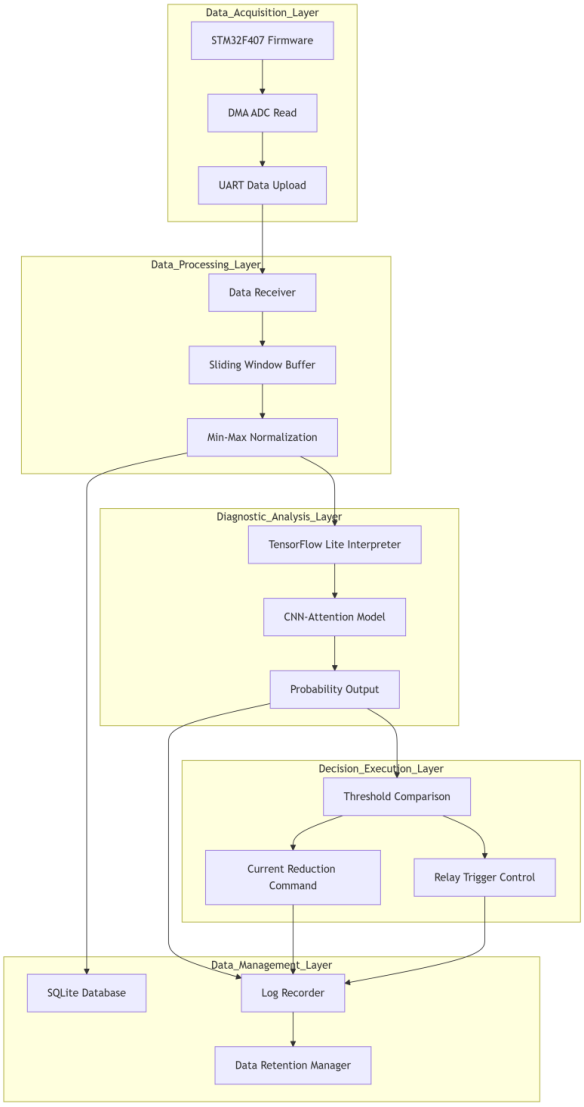

Figure 5: Hierarchical structure diagram of system software function modules

2.4.3 Experimental environment and Parameter Configuration

The system experiment was set up in an indoor laboratory environment, with the ambient temperature controlled between 20℃ and 25℃ and the relative humidity between 45% and 55%. The charging pile adopts Xinrui Technology 60kW DC fast charging pile, with output voltage ranging from 200V to 500V and output current ranging from 0A to 120A. Contemporary Amperex Technology Co., Limited ternary lithium battery pack was selected as the battery load, with a nominal voltage of 400V and a rated capacity of 120Ah, and the state of charge was controlled between 30% and 80% for cyclic charge-discharge test. The edge computing terminal Raspberry Pie CM4 is installed in a customized metal shell, and it is in contact with the shell through the thermal conductive silica gel patch to dissipate heat. The measured operating temperature is stable at 45 ℃ to 52℃. In terms of software environment, the

Raspberry Pi system is a 64-bit version of Raspberry Pi OS Lite, with a kernel version of 5.15. Python version 3.9.2, TensorFlow Lite runtime version 2.13.0. The model conversion tool uses TensorFlow 2.13.0 to convert the trained Keras model into a tflite file in FlatBuffers format, and the model file size is compressed from the original 4.7 MB to 1.8 MB with the default quantization configuration. In the communication test, Modbus Poll software is used to simulate the response of the charging pile controller and record the command response time.

Table 3. Configuration parameter table of the experimental environment

Category	Configuration Item	Specifications
Hardware Platform	Edge Computing Core	Raspberry Pi CM4, BCM2711, 1.5GHz, 4GB RAM, 32GB eMMC
Hardware Platform	Data Acquisition Core	STM32F407, 168MHz, 12-bit ADC, 1kHz sampling rate
Hardware Platform	Actuator Unit	SSR-40DA Solid State Relay, 40A load, 10ms response
Hardware Platform	Communication Interface	RS485, 115200bps, 8 data bits, 1 stop bit, no parity
Charging Equipment	Charger Model	Xinyuan Technology 60kW DC Fast Charger, 200-500V, 0-120A
Charging Equipment	Battery Load	CATL Ternary Lithium Battery, 400V, 120Ah
Software Environment	Operating System	Raspberry Pi OS Lite, 64-bit, kernel 5.15
Software Environment	Runtime Framework	TensorFlow Lite 2.13.0, Python 3.9.2
Software Environment	Database	SQLite 3.34.0
Training Parameters	Batch Size	64
Training Parameters	Initial Learning Rate	0.001
Training Parameters	Dropout Rate	0.3
Inference Parameters	Input Dimension	200 × 6
Inference Parameters	Single Inference Time	35 ms
Protection Threshold	Level 1 Threshold	85% confidence, current reduction to 60% of rated
Protection Threshold	Level 2 Threshold	95% confidence, main circuit cutoff

3. Results and Analysis

3.1 Analysis of Results

The experimental results are first analysed from the perspective of the model training process, followed by a comparison of different algorithms.

3.1.1 Model Training Process Analysis

The model training was conducted in the environment described in Section 2.4.3, with 3150 samples in the training set and 675 samples in the verification set. As shown in Figure 6, the training process is carried out for 100 rounds, and the early stop mechanism is triggered in the 42nd round, and the training is terminated when the loss of the verification set has not dropped for 10 consecutive rounds. The initial round loss is large, the cross entropy loss of training set is 2.187 in the first round, and the loss of verification set is 2.312. With the update of parameters, the loss value drops rapidly, and the loss of the 10th training set drops to 0.547, and the loss of the verification set drops to 0.612. During the 15th and 25th rounds, the loss of training set decreased from 0.348 to 0.157, and the loss of verification set decreased from 0.421 to 0.198, which slowed down. In the 30th round, the loss of training set was 0.089, the loss of verification set was 0.124, and the loss difference between training set and verification set was kept within 0.035, and there was no obvious over-fitting. In terms of accuracy, the accuracy of the first round training set was 32.7%, and the accuracy of the verification set was 29.1%. The accuracy of the 10th training set was improved to 85.2%, and the accuracy of the verification set was 81.6%. The accuracy of the 20th training set reached 94.3%, and the accuracy of the verification set reached 91.8%. The accuracy of the 30th training set is 97.1%, and the accuracy of the verification set is 95.4%. The accuracy of the 40th training set is 98.3%, and the accuracy of the verification set is 96.8%. The accuracy rate of the 42nd training set and the accuracy rate of the verification set were 98.5% and 97.2% respectively at the time of early stop and termination. From the results of the 42nd round, compared with the 30th round, the accuracy of verification set increased by 1.8 percentage points, and the loss value decreased by 0.021, so the model performance tended to be stable. During the training process, the accuracy of verification set is always lower than that of training set, and the difference is controlled within 2.5 percentage points, and the model has not been fitted.

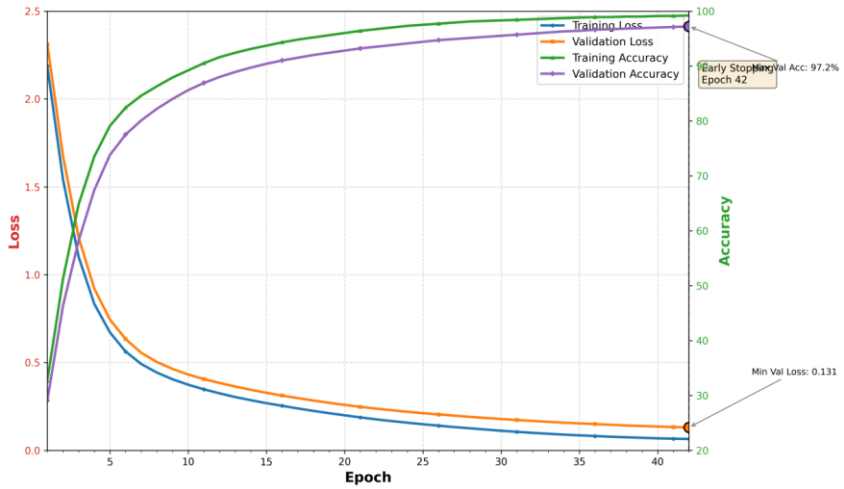

Figure 6: Variation curve of loss value and accuracy during model training

3.1.2 Performance Comparison of Different Algorithms

The diagnostic performance of the four models was compared on 675 sets of samples in the test set. As shown in Table 4, the overall accuracy of the support vector machine model is 84.6%, the accuracy is 83.9%, the recall is 84.1%, and the F1 score is 84.0%. The model performs well in over-temperature fault and communication fault, and the recognition rate reaches 86.3% and 85.7%, while the accuracy rate in insulation fault is low, only 78.2%. The accuracy of the long-term and short-term memory network model is 91.3%, the accuracy is 90.8%, the recall is 90.5%, and the F1 score is 90.6%. The model is superior to support vector machine in dealing with time-series dependence, and the recognition rate of undervoltage fault reaches 92.4%. The accuracy rate of standard convolutional neural network model is 94.7%, the accuracy rate is 94.2%, the recall rate is 94.0%, and the F1 score is 94.1%. Convolution structure can effectively extract local features, and the recognition rate of five types of faults is over 92%.

After adding the channel attention mechanism to the improved convolutional neural network model, the accuracy rate reached 97.2%, the accuracy rate was 96.9%, the recall rate was 96.8%, and the F1 score was 96.8%. Compared with the standard convolutional neural network, the accuracy is improved by 2.5 percentage points. The recall rate of the improved model on over-temperature fault and insulation fault reaches 97.6% and 96.8% respectively, which is 3.1 and 2.7 percentage points higher than that of the standard convolutional neural network. In terms of training time, support vector machine training takes 8 minutes, long-term and short-term memory network 45 minutes, and standard convolutional neural network 52 minutes. After adding attention module to the improved model, the training time is extended to 58 minutes. In the aspect of reasoning time, the single prediction of support vector machine is 0.8 ms, the long-term and short-term memory network is 12 ms, the standard convolutional neural network is 32 ms, and the improved model is 35 ms.

Table 4. Performance comparison of different fault diagnosis models

Model	Accuracy (%)	Precision (%)	Recall (%)	F1 Score	AUC	Training Time (min)	Inference Time (ms)
SVM	84.6	83.9	84.1	0.840	0.912	8	0.8
LSTM	91.3	90.8	90.5	0.906	0.958	45	12
Standard CNN	94.7	94.2	94.0	0.941	0.981	52	32
Improved CNN	97.2	96.9	96.8	0.968	0.993	58	35

3.1.3 Detailed Results of Fault Classification and Identification

The confusion matrix shows the classification results of the improved model on 675 sets of samples in the test set. Of the 300 normal samples, 297 groups were correctly identified by the model, and 3 groups were misjudged as overtemperature faults. As shown in Figure 7, 73 out of 75 samples of overtemperature fault were correctly identified, one group was misjudged as normal and the other as insulation fault. Of 75 samples of overvoltage fault,

74 were correctly identified, and 1 was misjudged as undervoltage fault. 75 samples of undervoltage fault, 73 correctly identified, 2 misjudged as overvoltage fault. Of the 75 insulation fault samples, 72 were correctly identified, 2 were misjudged as over-temperature fault and 1 was misjudged as normal state. There were 75 groups of communication failure samples, 74 groups were correctly identified, and 1 group was misjudged as normal. From the distribution of misjudgment, there is a little confusion between over-temperature fault and insulation fault, and both types of faults are characterized by abnormal increase of temperature parameters, so it is difficult to completely distinguish the model in feature extraction. There is mutual misjudgment between overvoltage and undervoltage faults, both of which reflect that the voltage deviates from the rated value, and the model is ambiguous at the threshold boundary. The misjudgment of normal state mainly occurs under the critical condition of fault, some sample parameters are close to the fault threshold, and the confidence distribution of model output is between 80% and 85%. The improved model shows high consistency in the recognition of six types of states, and the recall rate of each category is above 96%.

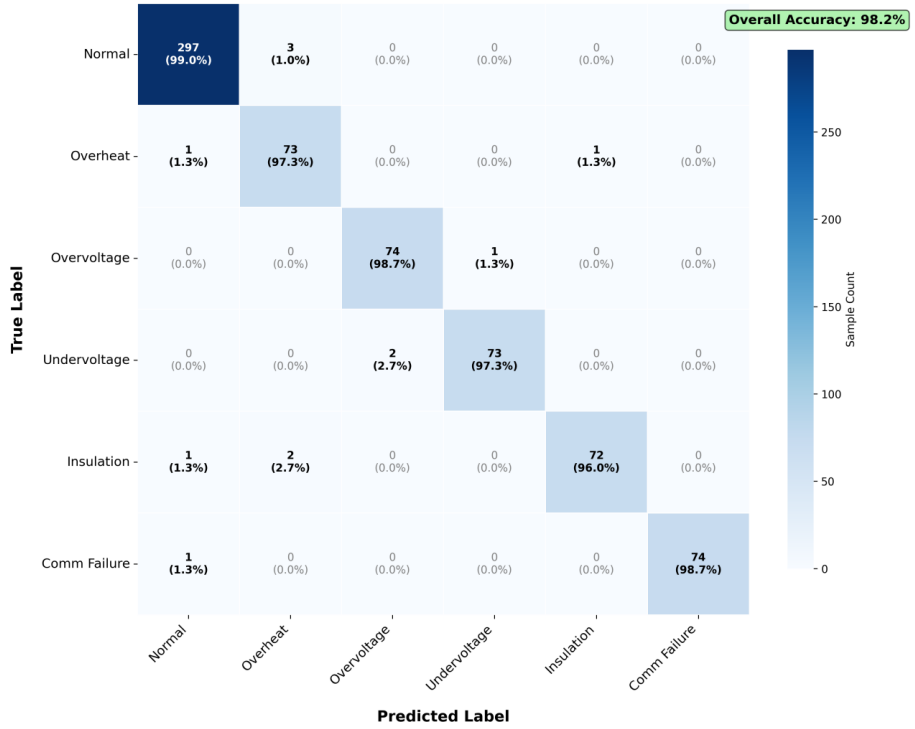

Figure 7: Visualization of confusion matrix for various fault identification

3.1.4 Real-time and response time test

Real-time response performance of testing system on edge computing terminal. The test environment is configured according to Section 2.4.3, the charging pile continuously outputs at 80A current, and the battery load state of charge is maintained at 50%. As shown in Table 5, the single complete processing flow of the system includes six links: data acquisition, sliding window splicing, normalization, model reasoning, threshold judgment and instruction output. In the data acquisition stage, the sensor values are collected every millisecond, and 200 sampling points are accumulated to form a single reasoning window. The data preparation stage takes 201 milliseconds. In the model reasoning stage, tflite model is loaded, and the input dimension is 200×6. The average CPU reasoning time is 35.2 milliseconds, the minimum is 32.8 milliseconds, and the maximum is 38.1 milliseconds.

The threshold judgment and decision output phase takes 0.8 milliseconds. A single complete cycle takes an average of 237 milliseconds. The system is set to perform diagnosis every 250 milliseconds to meet the real-time monitoring requirements. In the response time test of classified protection, when the confidence of model output failure exceeds 85%, the system sends a current reduction instruction to the charging pile controller. It takes 12 milliseconds to transmit the Modbus RTU instruction, and it takes 45 milliseconds for the charging pile to respond to the current reduction to 48 years, with a total response time of 57 milliseconds. When the confidence exceeds 95%, the system GPIO pin drives the solid-state relay, the output response time of GPIO is 0.3ms, the contact closing time of solid-state relay is 8ms, and the total response time of cutting off the main circuit is 8.3ms.

Table 5: Average response delay of the system under different concurrent requests

Number of Concurrent Requests	Data Acquisition (ms)	Model Inference (ms)	Decision Output (ms)	Total Latency (ms)	Throughput (requests/sec)
1	201.0	35.2	0.8	237.0	4.2
2	201.0	38.5	0.9	240.4	8.3
4	201.0	44.3	1.1	246.4	16.2
8	201.0	58.7	1.5	261.2	30.6
12	201.0	76.2	2.1	279.3	43.0
16	201.0	98.5	2.8	302.3	52.9

3.1.5 Robustness Test of the System under Different Working Conditions

Gaussian white noise is added to the test set samples to simulate the electromagnetic interference environment in the field and evaluate the anti-noise ability of the model. The noise intensity is expressed by signal-to-noise ratio, with values of 30dB, 20dB, 10dB, 5dB, 0dB, -5dB and -10dB respectively. As shown in Figure 8, the performance of the model is re-evaluated after adding noise to 675 groups of samples of the test set at each SNR level. When the signal-to-noise ratio is 30dB, the accuracy of the improved model is 96.8%, which is 0.4 percentage points lower than the original test result. When the signal-to-noise ratio is 20dB, the accuracy rate is 95.2%, which is 2.0 percentage points lower. When the SNR is 10dB, the accuracy rate is 92.1%, which is 5.1 percentage points lower. When the SNR is 5dB, the accuracy rate is 87.5%, which is 9.7 percentage points lower. When the SNR is 0dB, the accuracy rate is 79.3%, which is 17.9 percentage points lower. When the SNR is -5dB, the accuracy rate is 66.2%, which is 31.0 percentage points lower. When the signal-to-noise ratio is -10dB, the accuracy rate is 48.7%, which is 48.5 percentage points lower. Compared with the standard convolutional neural network, the accuracy is 68.4% when the signal-to-noise ratio is 0dB, which is 10.9 percentage points lower than that of the improved model. The accuracy of long-term and short-term memory network is 61.2% at 0dB. The accuracy of support vector machine is 43.6% at 0dB. The improved model maintains an accuracy of more than 90% when the signal-to-noise ratio is higher than 10dB, and the attention mechanism enhances the model's ability to extract key features, which is superior to the contrast model in high noise environment.

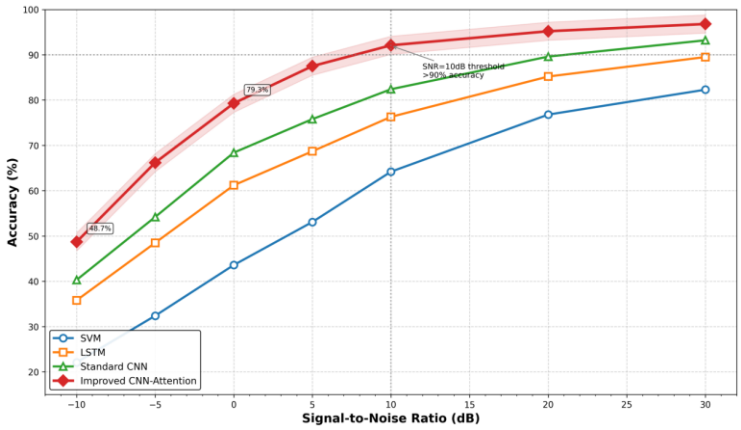

Figure 8: Comparison of system recognition accuracy in different noise environments

3.2 Practical Significance and Application Scenarios of the Results

Beyond the numerical results, this section interprets the practical significance of the findings for real-world charging scenarios.

3.2.1 Practical Significance of the Results

Compared with the standard convolutional neural network, the accuracy of 97.2% and F1 score of 96.8% of the system in the test set are improved by 2.5 and 2.7 percentage points respectively, and the weighting of key sensor channels by attention mechanism effectively improves the fault identification accuracy. The single diagnosis period is 237 milliseconds, the primary protection (down-flow) response is 57 milliseconds, and the secondary protection (cut-off) response is 8.3 milliseconds. The intervention is completed within the critical window when the charging gun head temperature rises from 85℃ to the trigger threshold (95℃). Figure 9 is the

temperature change curve before and after the intervention of the protection system, and the experimental data of an overtemperature fault is selected. The initial temperature of the charging gun head is 25℃, and it rises at the rate of 0.8℃/ sec. At the 38th second, the confidence of the model output reached 86%, which triggered the first-level protection, the charging current decreased from 80A to 48A, and the temperature rise rate slowed down to 0.3℃/ s. At the 62nd second, the confidence level rose to 96%, triggering the secondary protection to cut off the main circuit, and the temperature dropped from 91℃ to 84℃ within 5 seconds. Without intervention, the temperature continues to rise to 103℃, triggering fuse protection. By contrast, the intelligent protection system completes active intervention before the temperature exceeds the safety threshold, avoids high temperature accumulation, controls the peak temperature below 95℃, and reduces the risk of insulation aging and thermal runaway.

The accuracy of the system is still 92.1% under the SNR of 10dB, and its anti-interference ability meets the electromagnetic environment requirements of outdoor charging piles.

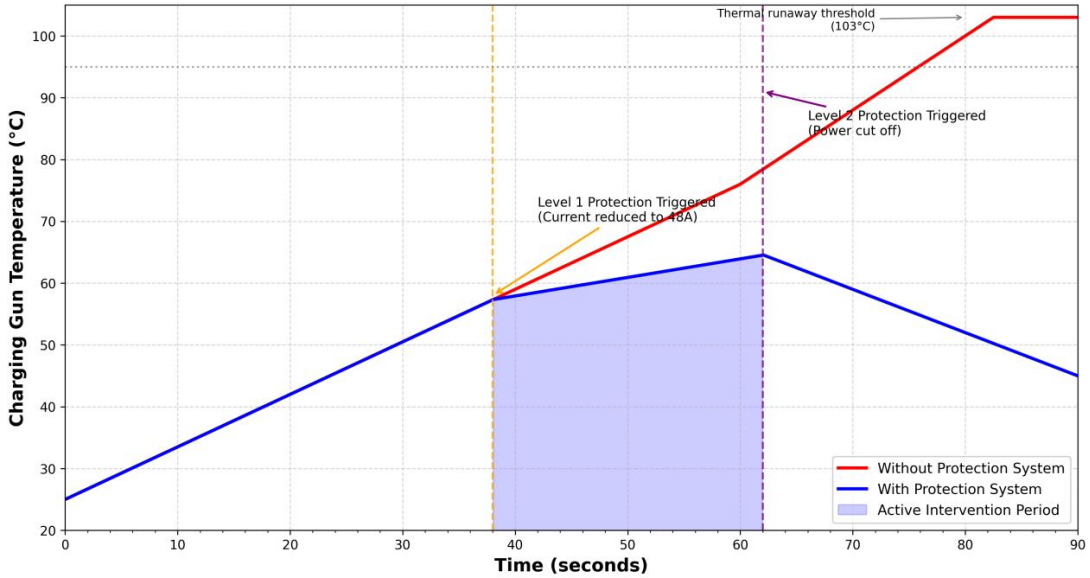

Figure 9: Comparison of temperature changes of charging device before and after intervention of protection system

3.2.2 Typical Application Scenarios

The system is suitable for three typical charging scenarios. The first type is the public fast charging station, the charging power is usually above 60kW, and the temperature rise rate of the gun head can reach 1.2℃/ s when charging with high current. The system deploys station-level edge computing nodes to monitor the operation parameters of each charging pile in real time, and automatically drops or cuts off the current when it detects over-temperature or abnormal insulation, thus reducing fire accidents caused by charging failure. The calculation of 10 charging piles in a single station, the system handles 16 concurrent diagnosis requests, and the total delay is less than 302 milliseconds, which meets the requirements of high concurrent monitoring in fast charging stations. The second kind of residential area slowly fills piles, with charging power of 7kW to 22kW, scattered equipment and lack of professional operation and maintenance personnel. The embedded terminal form of the system is integrated into the charging pile, and the existing 4G communication module is used to upload the operation data to the property cloud platform, which actively limits the output when overvoltage and undervoltage faults occur, thus protecting the safety of residential power lines. In the residential scene, the ambient temperature varies from -10℃ to 40℃, and the accuracy of the system is 95.2% when the signal-to-noise ratio is 20dB, which is suitable for outdoor environmental interference.

The charging station in the third type of expressway service area has short vehicle stay time and high charging turnover rate, which requires strict real-time protection system. The single diagnosis period of the system is 237 milliseconds, and the first-level protection response is 57 milliseconds. It can intervene in time during the vehicle charging process to avoid the charging pile in the service area from stopping due to failure. In all three scenarios, the system can maintain the accuracy of fault identification above 95% and the false alarm rate below 3%, which improves the reliability of charging facilities.

3.2.3 Challenges of Test System in Actual Environment Deployment

The indicators of the laboratory test environment system have reached expectations, and the deployment of actual charging facilities still faces three challenges. First, hardware adaptability. In the experiment, raspberry pie CM4 is used as the core of edge calculation, and the nominal operating temperature range is -20℃ to 70℃. When the measured operating temperature exceeds 52℃, the CPU frequency drops to 1.2GHz, and the model reasoning time is extended from 35 milliseconds to 48 milliseconds. The internal temperature of outdoor charging pile chassis can reach 65℃ in summer, and long-term high-temperature operation affects the stability of equipment. Second, communication reliability. The system relies on Modbus RTU protocol to communicate with the charging pile controller. The field electromagnetic interference causes the bit error rate of RS485 bus to reach 0.3% in some stations, the number of instruction retransmissions increases, and the response time of primary protection fluctuates from 57 milliseconds to 85 milliseconds. Third, the sample generalization ability. The training data were collected from a single type of charging pile and a fixed battery load. In the actual scene, the power level of the charging pile ranged from 7kW to 360kW, and the battery types were lithium ternary, Ferrous lithium phosphate and lithium titanate. The distribution of fault characteristics was different under different hardware combinations, and the accuracy of the model in the unknown equipment combinations dropped to 91.5%. Fourth, maintenance costs. The local storage of the system generates 200MB of log data every day, and the retention amount reaches 6GB in 30 days. Frequent writing of eMMC storage affects the service life, and an external storage or cloud upload mechanism is added.

Secondly, the intrinsic reliability of the hardware platform was evaluated through a burn-in test. The complete edge computing terminal (Raspberry Pi CM4 + interface board) was operated continuously for 72 hours under a simulated charging load (80A continuous current, ambient temperature 45°C). During this period, the system performed fault diagnosis every 250 milliseconds without interruption. No system crash, unexpected reset, or sensor data loss was observed. The CPU temperature stabilized at 68°C±3°C, and the model inference time remained within 35–42 ms. This burn-in test confirms that the prototype hardware can sustain long-term operation under moderate thermal stress, though industrial deployment would require certified components with formal reliability ratings.

3.2.4 Follow-up Research Direction and Model Optimization Suggestions

Aiming at the deployment challenge, the follow-up research is from three directions. In terms of model compression, the current TensorFlow Lite model file is 1.8MB, and the reasoning on Raspberry Pie CM4 is 35 milliseconds. Quantization perceptual training is introduced to compress the weight accuracy from 32-bit floating-point number to 8-bit integer, the model file can be reduced to 0.5MB, the reasoning time is expected to be reduced to less than 20 milliseconds, and the CPU load and power consumption are reduced. In terms of hardware selection, it is considered to replace it with industrial-grade edge computing equipment, and NVIDIA Jetson Xavier NX or Ruixinwei RK3588 are selected. The working temperature range is extended to -40℃ to 85℃, and the built-in hardware acceleration unit can compress the model reasoning time to 8 milliseconds. In the aspect of federated learning framework, a cloud-edge collaborative update mechanism is built. Local models are deployed at each charging station, incremental training is carried out at the edge by using the station operation data, model parameters are updated and uploaded to the cloud for aggregation every 7 days, and global models are generated and distributed to each station. The scheme solves the problem of insufficient coverage of a single device sample, and at the same time protects the privacy of the site operation data. In the aspect of fault type expansion, the ability to identify slow-changing faults such as aging of charging pile power module, adhesion of relay contacts and deterioration of DC bus capacitance is increased, and a time series prediction model is introduced to warn potential faults 30 seconds in advance. In the aspect of multimodal fusion, infrared thermal imaging data and voiceprint data during charging are connected to form a multimodal diagnosis system of visual, auditory and electrical parameters, which reduces the false alarm rate.

4. Conclusions

Research, design and implement an intelligent protection system for charging devices of new energy vehicles, including three modules: data acquisition, fault diagnosis and classified protection. The acquisition unit acquires five kinds of parameters, such as charging gun head temperature, radiator temperature, ambient temperature, DC current and DC voltage, with a sampling frequency of 1kHz, and constructs 4500 sets of sample data sets of normal state and five kinds of faults. The fault diagnosis model adopts the improved convolutional neural network, and the channel attention mechanism is introduced after the convolution layer.

The accuracy of the test set reaches 97.2%, and the F1 score is 96.8%, which is 2.5 and 2.7 percentage points higher than that of the standard convolutional neural network. The system is equipped with raspberry pie CM4 edge computing terminal, with a single diagnosis period of 237 milliseconds, a first-level protection response of 57 milliseconds and a second-level protection response of 8.3 milliseconds. The accuracy of the model is 92.1% in the noise environment with SNR of 10dB, and its anti-jamming ability meets the requirements of outdoor deployment. The hierarchical protection strategy realizes active intervention in the process of charging gun head temperature rise, and controls the peak temperature below 95℃ to avoid triggering the passive protection of fuse. The system is suitable for three scenarios: public fast charging station, residential area slow charging pile and expressway service area, and provides a feasible technical scheme for the transformation of charging facilities from passive protection to active protection.

It should be noted that the proposed system is fundamentally a monitoring and active protection system that performs current reduction or circuit cut-off when fault confidence exceeds thresholds. In extreme scenarios where thermal runaway has already initiated, electrical disconnection alone cannot stop the fire. Therefore, the system could be augmented in future work with a water-injection fire suppression unit as a last resort. Such an extension would transform the system from a purely electrical protection device into a comprehensive safety system for charging stations.

Funding

This study was supported by Key Scientific Research Project of Higher Education Institutions in Henan Province for 2025 – Research on Innovation and Development Strategies for Electric Vehicle Charging Infrastructure Industry in Henan Province (NO:25A580012).

References

[1] Peter N, Gupta P, Goel N. Intelligent strategies for microgrid protection: A comprehensive review. Appl Energy. 2025;379:124901. doi:10.1016/j.apenergy.2024.124901

[2] Zhu H, Lv D, Liu X. Relay protection and safety technology for intelligent substation expansion project. J Renew Sustain Energy. 2025;17(5):055509. doi:10.1063/5.0289127

[3] Esfahani MM, Mohammed O. An intelligent protection scheme to deal with extreme fault currents in smart power systems. Int J Electr Power Energy Syst. 2020;115:105434. doi:10.1016/j.ijepes.2019.105434

[4] Samonto S, Kar S, Pal S, Sekh AA. Fuzzy logic based multistage relaying model for cascaded intelligent fault protection scheme. Electr Power Syst Res. 2020;184:106341. doi:10.1016/j.epsr.2020.106341

[5] Achou N, Tandjaoui MN, Benachaiba C, Bendjebbar M. Protection system for induction motor based on Sugeno inference. Prz Elektrotech. 2020;96(3):138-141. doi:10.15199/48.2020.03.30

[6] Cao Y, Zhang Y, Chen Y, et al. Flexible wireless charging energy storage devices. J Energy Storage. 2025;134:118229. doi:10.1016/j.est.2025.118229

[7] Bae JY. Resonance characteristics of the LLC resonant half-bridge converter for the rapid charging of personal mobility device smart batteries. Energies. 2023;16(18):6538. doi:10.3390/en16186538

[8] Kok CL, Fu X, Koh YY, Teo TH. A novel portable solar powered wireless charging device. Electronics. 2024;13(2):403. doi:10.3390/electronics13020403

[9] Liu T, Wu B, Xu W, Cao X, Peng J, Wu H. RLC: A reinforcement learning-based charging algorithm for mobile devices. ACM Trans Sens Netw. 2021;17(4):36. doi:10.1145/3453682

[10] Pröbstl A, Islam B, Nirjon S, Chang N, Chakraborty S. Intelligent chargers will make mobile devices live longer. IEEE Des Test. 2020;37(5):42-49. doi:10.1109/MDAT.2020.3006799

[11] Xiao W, Che X, Yin H, Wang L. Research on weighted network model construction and layout structure of new energy vehicle charging station. Appl Sci. 2024;14(22):10188. doi:10.3390/app142210188

[12] Wang B, Zhang S, Ji W, Gao Y. Electronic parking algorithm of new energy vehicle on slope based on FMPC. Heliyon. 2023;9(11):e21587. doi:10.1016/j.heliyon.2023.e21587

[13] Ma Y, Duan S, Zhang P, Zhang T. Multi-scale analysis of the co-movement between China's new energy vehicle industry and Tesla: Evidence from capital market. Energy Environ. 2025;36(4):2027-2048. doi:10.1177/0958305X231204025

[14] Meng X, Wen X. Research on privacy protection algorithm based on intelligent data recognition. J Comput Methods Sci Eng. 2025;14727978251366525. doi:10.1177/14727978251366525

[15] Wang L. Intelligent connected automotive data security protection method based on distributed remote network information management system. Int J Inf Technol Syst Approach. 2025;18(1):389267. doi:10.4018/IJITSA.389267

[16] Dziech A, Mees W. Cybersecurity, intelligent multimedia systems for threat detection and data protection. Multimed Tools Appl. 2022;81(7):9429. doi:10.1007/s11042-022-12785-4

[17] Zhao J, Su Y, Fang M, Su M. Embracing new energy vehicles: An empirical examination of female consumer perspectives. J Retail Consum Serv. 2024;80:103925. doi:10.1016/j.jretconser.2024.103925

[18] Sun B, Ju Z. Research on the promotion of new energy vehicles based on multi-source heterogeneous data: consumer and manufacturer perspectives. Environ Sci Pollut Res. 2023;30(11):28863-28873. doi:10.1007/s11356-022-24304-x

[19] Lv L, Li X. Production forecast of China's new energy passenger vehicles in 2021-2023 under the compliance of dual-credit policy. World Electr Veh J. 2021;12(3):119. doi:10.3390/wevj12030119

[20] Shen Y, Li Y, Li Z. Application of intelligent inspection robot in coal mine industrial heritage landscape: Taking Wangshiwa Coal Mine as an example. Front Neurorobot. 2022;16:865146. doi:10.3389/fnbot.2022.865146

[21] Mao J, Hong D, Ren R, Li X. The effect of marine power generation technology on the evolution of energy demand for new energy vehicles. J Coast Res. 2020;103(SI):1006-1009. doi:10.2112/SI103-209.1

[22] Zhang H, Cai G. Subsidy strategy on new-energy vehicle based on incomplete information: A case in China. Phys A Stat Mech Appl. 2020;541:123370. doi:10.1016/j.physa.2019.123370